J. Synchrotron Rad. (1998). **5**, 750–752

Nanosecond-resolved XMCD on ID24 at the ESRF to investigate the element-selective dynamics of magnetization switching of Gd–Co amorphous thin film

M. Bonfim,[a] K. Mackay,[a] S. Pizzini,[a] A. San Miguel,[b] H. Tolentino,[a] C. Giles,[b] T. Neisius,[b] M. Hagelstein,[b] F. Baudelet,[c] C. Malgrange[b,d] and A. Fontaine[a,b]*

[a]LLN, CNRS, BP 166, 38042 Grenoble CEDEX, France, [b]ESRF, BP 220, 38043 Grenoble CEDEX, France, [c]LURE, CNRS-CEA-MEN, 91405 Orsay CEDEX, France, and [d]Laboratoire de Minéralogie-Cristallographie, Université Paris 6 et 7, 75252 Paris CEDEX 05, France. E-mail: fontaine@labs.polycnrs-gre.fr

(*Received 4 August 1997; accepted 24 November 1997*)

The one-bunch filling mode of the ESRF is combined with a microcoil to generate a pulsed-magnetic-field pump phased with respect to the probe that is given by the bunch of photons emitted each turn (357 kHz). Nanosecond-resolved X-ray magnetic circular dichroism (XMCD) is carried out. Besides the microcoil, the two other key-elements are the energy-dispersive XAS spectrometer, which yields parallel data acquisition, and the diamond-based quarter-wave plate, which tunes the helicity of the photon alternatively left and right.

Keywords: time-resolved XMCD; quarter-wave plates; pump–probe schemes; energy-dispersive XAS spectrometers.

1. Experimental set-up

The dynamics of magnetization switching is an essential issue in recording technology (Freeman, 1994; Sun *et al.*, 1993). X-ray magnetic circular dichroism (XMCD) is a unique element-selective orbital-symmetry-selective spectroscopy. It has been enriched by the addition of the time resolution thanks to microcoils which generate pulses of magnetic field as large as 1 T at the 357 kHz ESRF frequency. The pump (magnetic field of a few nanoseconds)–probe (100 ps X-ray pulse processed by an energy-dispersive X-ray absorption spectrometer) scheme has been implemented, taking advantage of the single-bunch filling mode at the ESRF which opens up a tunable delay between pump and probe pulses from zero up to 2.8 μs. (Fig. 1). XMCD is collected by a stroboscopic approach which clearly means that we are dealing with reproducible magnetic states. Within the typical 3 min data-collection time, to build one XMCD spectrum at the Gd *L*-edge more than 6×10^7 X-ray pulses have been used.

The use of an ultrafast electroacoustic chopper, based on the diffraction of the surface acoustic waves generated on a multi-layer-coated $LiNbO_3$ crystal developed by Tucoulou *et al.* (1997), enables us to enlarge the accessible window for adjusting delays of the pump with respect to the probe, larger than the revolution period (2.8 ps).

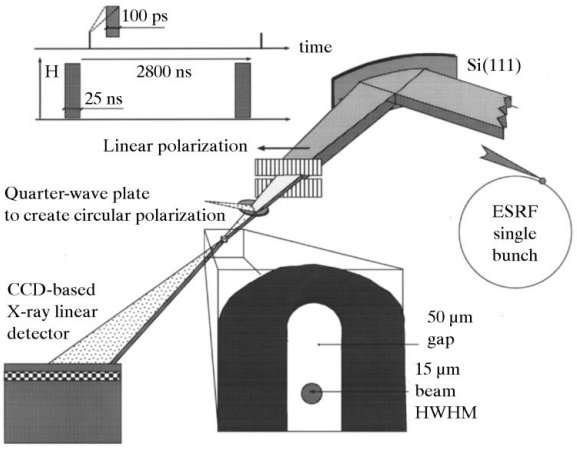

Figure 1
Schematic layout of the energy-dispersive XAS experimental station at the ESRF, with the implementation of the pump, presently a microcoil able to generate pulses of magnetic field at the ESRF frequency (357 kHz).

1.1. *The pump: magnetic field generated by a copper microcoil*

The hair-pin-shaped 50 μm-thick chemically processed copper microcoil with a 50 μm-wide gap takes full advantage of the focusing optics (a spot size as small as 30 × 100 μm) of the energy-dispersive XAS spectrometer of ID24. Typically, 25 ns-long pulses of 100 A current generate 0.4 T-high magnetic field pulses at the 357 kHz frequency (f) of the ESRF. Since the power delivered by the supply is limited, 10 ns-long pulses lead to a magnitude of 1 T with the repetition rate of the ESRF. At such a frequency the current penetration in copper is controlled by the skin depth, which is $f^{-1/2}$ dependent. The main technological issue is dealing with the temperature rise, which varies as $H^2/8C_v$, where C_v is the volumic heat of copper and H is the magnetic field. For 10 ns pulses at 357 kHz, $\Delta T \simeq 30H^2$ (H in T) which is still acceptable.

1.2. *The probe*

The energy-dispersive XAFS spectrometer is a key aspect of this approach to time-resolved phenomena since all the data

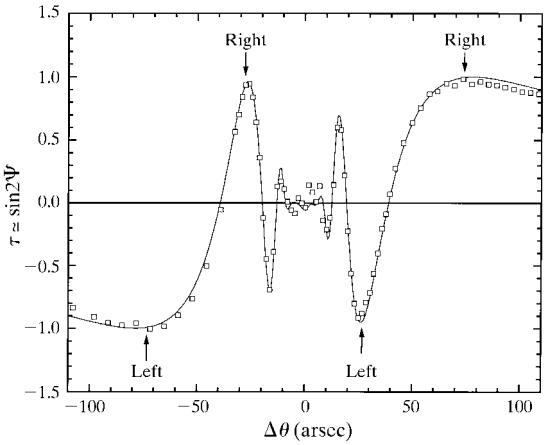

Figure 2
The measured evolution of the polarization rate *versus* the offset of the position of the diamond crystal with respect to the Bragg angle. The dynamical theory fits perfectly the experimental data provided that a 4.5 arcsec-wide convolution is used to account for the divergences (vertical and horizontal) of each monochromatic part of the polychromatic X-ray pass band, Bragg reflected by the bent Si(111) crystal. The QWP is a 707 μm-thick diamond crystal set close to the (111) reflection in the Laue geometry.

points of the whole spectrum are collected in parallel. The energy-dispersive spectrometer of ID24 uses a planar undulator as a source and the optics combine a Kitpatrick–Baez double-mirror configuration and a Bragg dispersing geometry which altogether focus the polychromatic beam to a spot size as small as 30 × 100 μm (Hagelstein *et al.*, 1998). The full spectrum of the transmitted beam is collected by a CCD-based position-sensitive detector in a few tens of milliseconds due to the typical flux of 5×10^{10} photons s^{-1} focused on the sample in the single-bunch mode.

The last optical element is the quarter-wave plate (QWP) which was implemented on ID24 last year to tune the photon helicity from left-handed to right-handed at will in less than 1 s (Giles *et al.*, 1994). Thanks to the high quality of diamond crystals, the birefringent properties in the vicinity of a Bragg reflection are able to transform X-rays with the natural horizontal polarization produced by the flat undulator into circular-polarized photons. In addition, flipping from one side of the diamond (111) Bragg peak to the other allows the helicity to be tuned from left to right with a circular polarization rate close to 1 (0.99 at 7243 eV, the Gd L_3-edge energy). The XMCD signal originates from the difference of absorption for similar photons of two helicities. This approach to collecting the XMCD signal is unusual in most experimental stations throughout the world, even though it fits the original definition of circular dichroism. Let us recall, however, that on ID12 at the ESRF such a scheme is currently operated: the helicity flipping comes from the phase shift of one jaw of the helical undulator with respect to the other. Otherwise the XMCD signal comes currently from the inversion of the direction of the magnetization, which limits the XMCD study to saturated or hysteresis-free systems.

Fig. 2 is the measured evolution of the polarization rate *versus* the offset of the position of the diamond crystal with respect to the Bragg angle of the diamond. The energy-dispersive Bragg optics of the polychromator add an additional constraint which is easily overcome. The dynamical theory fits perfectly the experimental data provided that a 4.5 arcsec-wide convolution is used to account for the divergences (vertical and horizontal) of each monochromatic part of the polychromatic X-ray pass band, Bragg reflected by the bent Si(111) crystal. The QWP is a 707 μm-thick diamond crystal set close to the (111) reflection in the Laue geometry.

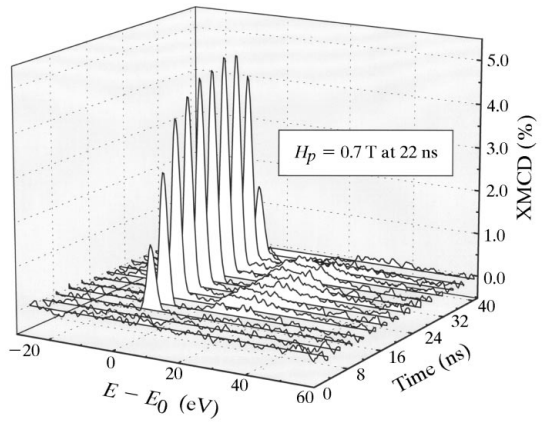

Figure 3
The three-dimensional plot shows the XMCD response of the Gd–Co amorphous film at the Gd L_3-edge, recorded all along the 22 ns-wide 0.7 T-high magnetic field pulse and after. The probe is given by the bunch of photons, about 100 ps long, processed by the optics (mirrors, Bragg polychromator, *i.e.* bent Si crystal and the QWP).

2. Investigated systems

The first study dealt with Gd–Co_3 amorphous thin film, which saturates at about 0.5 T. The film is slightly anisotropic with an easy axis of magnetization in the plane of the film. In the experiment the field produced by the microcoil was applied perpendicular to the film, along the X-ray propagation direction. Therefore the issue which is addressed is the dynamics of the rotation of the magnetization from the planar to the perpendicular direction to the film. The XMCD signal at the Gd L_3-edge, which originates from the difference of absorption after the QWP-controlled helicity flipping, gives the Gd dynamical response. Using the same set-up to generate field pulses we investigated the Kerr response of this amorphous Gd–Co_3, which is mostly due to the spin polarization of the shallow 3*d* bands of cobalt.

Fig. 3 show the XMCD signals recorded at different times along the pulse (0.7 T maximum, 22 ns wide) and all the way down and after the pulse. Each signal is the result of 3 min of data collection with a dead time of about 30% (five helicity flippings and 11 image readouts and digitalization for each) which leaves room for improvement of the signal-to-noise ratio. The XMCD signal-to-noise ratio is over 100 in the best case. It is of the order of 10^4 for the absolute cross section.

Fig. 4 shows the superposition of the field pulses and the XMCD samplings for two magnitudes of the field pulse (0.35 T and 0.7 T). The Gd magnetization follows the profile of the field pulses with no delay as long as saturation is not reached. Therefore, we learn that the rotation of the Gd sublattice in this amorphous film is faster than 1 ns.

The next investigation should involve Th–Fe multilayers which show two regimes according to the Kerr data: a partly reversible behaviour and a long slow route (ns) back to zero magnetization.

3. Conclusions

The conclusions are mostly on the instrumental aspects: the time-resolved XMCD coupled to the single-bunch-mode operation at the ESRF is under control. The dynamics of the rotation of the Gd sublattice of the amorphous film are faster than 1 ns. The possible coupling between the sample and the coil has to be clarified by further investigations. It is clear from this first report that the

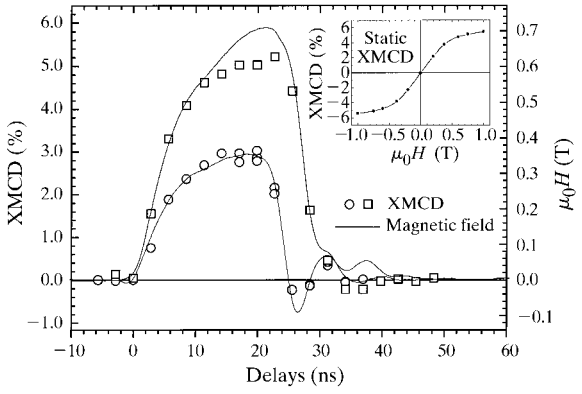

Figure 4
The time-dependent XMCD signal is compared with the profile of the field pulses. In the insert the static XMCD response is shown. For low field the response is linear.

stroboscopic approach should produce new insights into the magnetization switching thanks to the microcoil technology phased to the ESRF bunch and thanks to the operation of a diamond-based QWP to tune rapidly the photon helicity.

References

Freeman, M. R. (1994). *J. Appl. Phys.* **75**, 6194–6198.

Giles, C., Malgrange, C., Goulon, J., Vettier, C., de Bergevin, F., Dartyge, E., Fontaine, A., Giorgetti, C. & Pizzini, S. (1994). *J. Appl. Cryst.* **27**, 232–240.

Hagelstein, M., Lienert, U., Ressler, T., San Miguel, A., Freund, A., Cunis, S., Schulze, C., Fontaine, A. & Hodeau, J.-L. (1998). *J. Synchrotron Rad.* **5**, 753–755.

Sun, C. K., Vallée, F., Acicoli, L., Ippen, E.-P. & Fujimoto, J.-G. (1993). *Phys. Rev. B*, **48**, 12365.

Tucoulou, R., Roshchupkin, D. V., Schelovkov, I. A., Brunel, M., Ortega, L., Ziegler, F., Lingham, M., Mouget, C. & Douillet, S. (1997). *Nucl. Instrum. Methods*, B**132**, 207–213.